Topology Optimization of Magnetic Cores for WPT Using the Geometry Projection Method

*, †Yoshitsugu Otomo and *Hajime Igarashi
*Graduate School of Information Science and Technology, Hokkaido University, Sapporo 060-0814, Japan
†Research Fellow of Japan Society for the Promotion of Science (JSPS), Tokyo 102-0083, Japan

***Purpose*—**The purpose of this study is to search for an optimal core shape that is robust against misalignment between the transmitting and receiving coils of the wireless power transfer (WPT) device. During the optimization process, we maximize the coupling coefficients while minimizing the leakage flux around the coils to ensure the safety of the WPT device.

***Design/methodology/approach*—**In this study, a novel topology optimization method for WPT devices using the geometry projection method is proposed to optimize the magnetic core shape. This method facilitates the generation of bar-shaped magnetic cores because the material distribution is represented by a set of elementary bars.

***Findings*—**It is shown that an optimized core shape, which is obtained through topology optimization, effectively increases the net magnetic flux interlinked with the receiving coil and outperforms the conventional core.

***Originality/value*—**In the previous topology optimization method, the material distribution is represented by a linear combination of Gaussian functions. However, this method does not usually result in bar-shaped cores, which are widely used in WPT. In this study, we propose a novel topology optimization method for WPT devices using geometry projection that is used in structural optimization, such as beam and cantilever shapes.

***Index Terms*—Geometry projection method, Robust optimization, Topology optimization, Wireless power transfer (WPT).**

I. Introduction

Wireless power transfer (WPT) has been widely used in various electric devices, ranging from electric vehicles and airplanes to smartphones [1]. WPT devices are required to have high efficiency, even when the transmitting and receiving coils are misaligned. The magnetic cores are placed in the vicinity of the coils to improve efficiency. They must be as small as possible to reduce the manufacturing cost and device size. In addition, the leakage flux around the coils must be reduced to limit the electromagnetic field exposure to the human body. For such WPT devices, parameter optimization methods for bar-shaped and H-shaped magnetic cores have been proposed [2]–[4]. These approaches require the setting of adequate parameters, which rely on the insights of experienced engineers. Moreover, it is difficult to find novel bar structures that lead to an improvement in efficiency by using this approach.

In contrast to conventional parameter optimization, topology optimization, which does not need a pre-setting of the design parameters, can lead to novel structures. In particular, topology optimization, in which the material distribution is represented by a linear combination of Gaussian functions, has been proven to be effective for the design of electric motors and WPT devices [5]–[7]. However, this method typically does not result in bar-shaped cores, which are widely used in WPT. This is because a small change in the weighting coefficients of Gaussian functions can separate the bar-shaped core into segments.

In this study, we propose a novel topology optimization method for WPT devices using geometry projection, which is used in structural optimizations such as beam and cantilever shapes [8]–[10]. This method facilitates the generation of bar-shaped magnetic cores because the material distribution is represented by a set of elementary bars. In this study, we adopt a real-coded genetic algorithm (GA) to determine the optimal distribution and shape of the elementary magnetic bars. Moreover, we search for an optimal solution that is robust against misalignment between the transmitting and receiving coils. The proposed method is compared with the topology optimization method based on Gaussian functions.

The remainder of this paper is organized as follows. In section II, we describe the topology optimization method based on the geometry projection method and Gaussian functions. In section III, we define the optimization problems by considering the coupling efficiency and leakage flux. In section IV, we discuss the optimization results obtained by using the two methods. Finally, section V concludes the paper with a concise summary of this study.

II. Optimization Methods

A. Geometry Projection Method

In topology optimization using the geometry projection method [8], the magnetic core shape is represented by elementary bars, as shown in Fig. 1. Each elementary bar is parameterized based on the location of the end points of its medial axis, $\boldsymbol{x}_{\mathrm{o}}$, $\boldsymbol{x}_{\mathrm{f}}$, and its radius, r_{b}, as shown in Fig. 1(a). We assume that all elementary bars have the same r_{b} value for simplicity, although they can be treated as one of the optimization variables. The material attribute, M_e, of finite element e in the design region, Ω_{core}, is determined by projecting the elementary bars onto finite element e as follows:

This work was supported in part by the JSPS KAKENHI under Grant JP19J20375 and in part by the MEXT D-DRIVE-HU program.

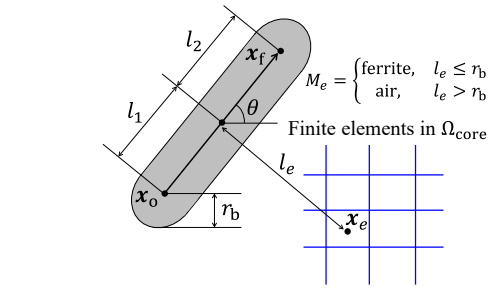

(a) Elementary bar

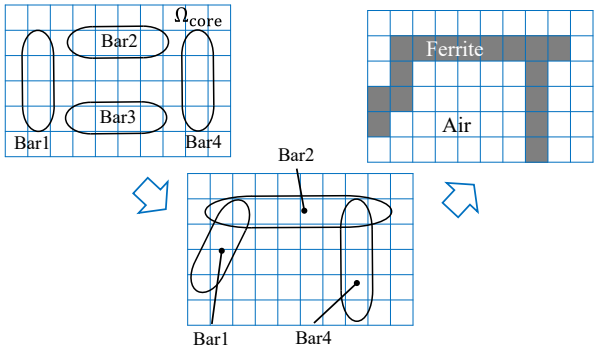

(b) Schematic of geometry projection

Fig. 1. Geometry projection method

$$M_e = \begin{cases} \text{ferrite}, & l_e \le r_b \\ \text{air}, & l_e > r_b \end{cases}, \tag{1}$$

where l_e denotes the distance between the center of element $\boldsymbol{x}_e$ and medial axis of the cylindrical bars. The geometry projection is schematically shown in Fig. 1(b). First, we uniformly arrange the elementary bars in the design region, Ω_{core}. Then, lengths l_1 and l_2 and rotation angle θ of each elementary bar are determined. Finally, the material properties are assigned to all elements mentioned in (1) according to the distribution of the elementary bars. After completing the aforementioned process, we solve the following magnetostatic equation to evaluate the objective function:

$$\text{rot}\, \nu\, (\text{rot}\, \boldsymbol{A}) = \boldsymbol{J}\,, \tag{2}$$

where ν, $\boldsymbol{A}$, and $\boldsymbol{J}$ denote the magnetic reluctivity, vector potential, and current density, respectively. The FE discretization of (2) leads to

$$\sum_j A_j \int_\Omega \text{rot}\, \boldsymbol{N}_i\, \nu \left(\text{rot}\, \boldsymbol{N}_j\right) d\Omega = \int_{\Omega_{\text{coil}}} \boldsymbol{N}_i \cdot \boldsymbol{J}\, d\Omega\,, \tag{3}$$

where $\boldsymbol{N}_i$ denotes the vector interpolation function.

In the optimization, the geometrical parameter vector, $\boldsymbol{p} = \left[l_1^1, \ldots, l_1^Q,\ l_2^1, \ldots, l_2^Q,\ \theta^1, \ldots, \theta^Q\right]^{\text{t}} \in \mathbb{R}^{3Q}$is determined to maximize the objective function by employing the real-coded GA [11] subjected to given constraints, where the superscript in $\boldsymbol{p}$ running from 1 to Q identifies the elementary bars.

B. On/Off Method Based on NGnet

In the topology optimization using the normalized Gaussian network (NGnet) [5], which is schematically

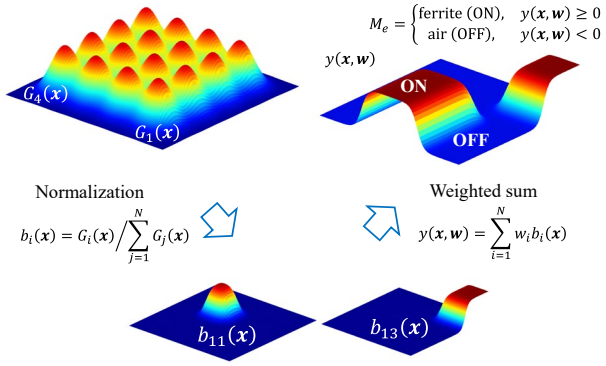

Fig. 2. On/off method using normalized Gaussians

shown in Fig. 2, the material attribute in the design region, Ω_{core}, is determined from the value of the shape function defined by

$$y(\boldsymbol{x},\boldsymbol{w}) = \textstyle\sum_{i=1}^{N} w_i b_i(\boldsymbol{x}), \tag{4}$$

where w_i and N denote the weighting coefficient and number of Gaussian functions, respectively. Moreover, the normalized Gaussian function, $b_i(\boldsymbol{x})$, is given by

$$b_i(\boldsymbol{x}) = G_i(\boldsymbol{x}) / \textstyle\sum_{j=1}^{N} G_j(\boldsymbol{x}), \tag{5}$$

$$G_i(\boldsymbol{x}) = \frac{1}{2\pi\sigma^2} \exp\left\{-\frac{1}{2\sigma^2} |\boldsymbol{x} - \boldsymbol{x}_i|^2\right\}, \tag{6}$$

where σ and $\boldsymbol{x}_i$ denote the standard deviation and center of the Gaussian basis, respectively. The material attribute, M_e, of the finite element e in the design region, Ω_{core}, is determined as

$$M_e = \begin{cases} \text{ferrite}, & y(\boldsymbol{x},\boldsymbol{w}) \ge 0 \\ \text{air}, & y(\boldsymbol{x},\boldsymbol{w}) < 0. \end{cases} \tag{7}$$

The material distribution is determined by using (7), and (3) is solved to obtain the magnetic field and WPT performance.

In the optimization, the weighting coefficient vector, $\boldsymbol{w} = [w_1, w_2, \ldots, w_N]^{\text{t}} \in \mathbb{R}^N$, is determined to maximize the objective function by applying the GA.

III. Optimization Problems

A. Single-Objective Optimization

In single-objective topology optimization, we maximize the coupling coefficients of a WPT device for electric vehicles (EVs) considering misalignment between coils for robustness. Although the misalignment in the forward direction (y-axis) of EVs is easily limited by using a wheel stopper, it is difficult to limit the misalignment in the lateral direction (x-axis) [12]. For this reason, we focus on the lateral misalignment. Moreover, it is desirable to reduce the core volume to the maximum possible extent to reduce the cost and size. Thus, the optimization problem considering the robustness is defined by

TABLE I
SPECIFICATIONS OF OPTIMIZATION MODEL

Relative permeability	3300
Driving frequency	85 kHz
Inner radius of coils	100 mm
Outer radius of coils	150 mm
Number of coil turns	10
Input current for transmitting coil	20 A_{RMS}
Air gap	70 mm
Misalignment (*x*-direction)	200 mm

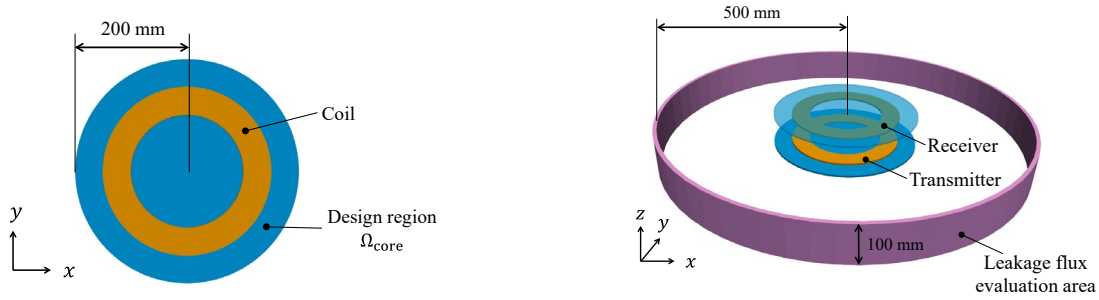

(a) Coil and design region

(b) Bird's-eye view of whole system

Fig. 3. Optimization model

(a) 16 (4×4) elementary bars. (range of bar length l_1 and l_2: 0 to 50 mm, bar radius r_b: 7.5 mm)

(b) 48 Gaussian functions (standard deviation σ: 1.7 mm). Note that the spheres' radius is standard deviation

Fig. 4. Distribution of elementary bars and Gaussian functions for the transmitting coil

Problem 1:

$$\max_{\boldsymbol{d}} F_1(\boldsymbol{d}), \quad F_1(\boldsymbol{d}) = \frac{1}{2}[k_1(\boldsymbol{d}) + k_2(\boldsymbol{d})] \quad \text{sub. to } V_{\text{core}} \le V_{\text{ref}} \tag{8}$$

where $k_1(\boldsymbol{d})$, $k_2(\boldsymbol{d})$, V_{core}, and V_{ref} denote the coupling coefficients under the alignment and misalignment conditions, total volume of the optimized core, and upper volume limit, respectively. We impose the volume constraint in (8) using the oracle penalty method [13]. In (8), $\boldsymbol{d}$ represents the design variable of the optimization methods expressed by (1) and (7). Based on the assumption that the transmitting and receiving coils have the same self-inductance, the coupling coefficient, $k_i(\boldsymbol{d})$, is obtained from the FE analysis as follows [14]:

$$k_i(\boldsymbol{d}) = \frac{\Phi_2^i}{\Phi_1^i} = \frac{\int_{\Omega\text{coil2}} \boldsymbol{A}_i(\boldsymbol{d}) \cdot \boldsymbol{j}_2 \, d\Omega}{\int_{\Omega\text{coil1}} \boldsymbol{A}_i(\boldsymbol{d}) \cdot \boldsymbol{j}_1 \, d\Omega}, \quad (i = 1, 2) \tag{9}$$

where $\boldsymbol{A}_i(\boldsymbol{d})$, Φ_m^i, and $\boldsymbol{j}_m$ $(m = 1, 2)$ denote the vector potential and magnetic flux for the alignment and misalignment conditions and the unit vectors parallel to the currents along the transmitting and receiving coils, respectively. Note that the vector potential, $\boldsymbol{A}_i(\boldsymbol{d})$, is an implicit function of the design variable, $\boldsymbol{d}$, because the magnetic field depends on the material distribution determined from $\boldsymbol{d}$.

B. Multi-Objective Optimization

In the multi-objective optimization, we maximize the coupling coefficients while minimizing the leakage flux around the coils to ensure the safety of the WPT device. The multi-objective optimization problem is defined as follows.

Problem 2:

$$\max_{\boldsymbol{d}} F_1(\boldsymbol{d}), \quad F_1(\boldsymbol{d}) = \frac{1}{2}[k_1(\boldsymbol{d}) + k_2(\boldsymbol{d})]$$
$$\min_{\boldsymbol{d}} F_2(\boldsymbol{d}), \quad F_2(\boldsymbol{d}) = \frac{1}{2}\left[B_1^{\text{leak}}(\boldsymbol{d}) + B_2^{\text{leak}}(\boldsymbol{d})\right] \tag{10}$$

Here, $B_1^{\text{leak}}(\boldsymbol{d})$ and $B_2^{\text{leak}}(\boldsymbol{d})$ denote the magnitude of the leakage flux density at the evaluation points under the alignment and misalignment conditions, respectively. Note that $B_1^{\text{leak}}(\boldsymbol{d})$ and $B_2^{\text{leak}}(\boldsymbol{d})$ are the implicit functions of the design variable, $\boldsymbol{d}$.

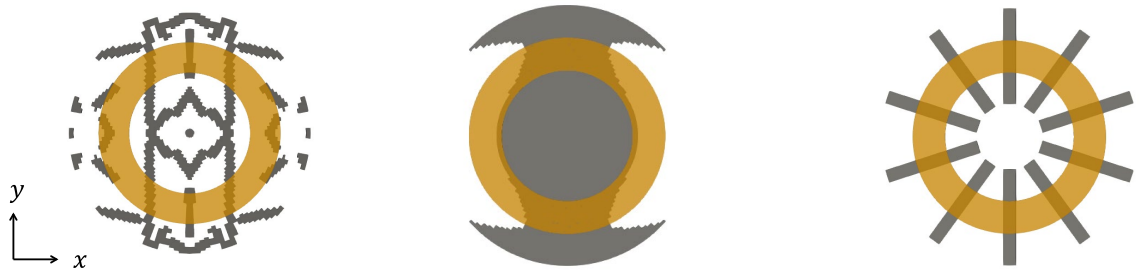

(a) Optimized (Geometry projection) ($k_1 = 41.5\ \%, k_2 = 5.0\ \%, V_{\mathrm{core}} = 0.65V_{\mathrm{ref}}$)

(b) Optimized (NGnet) ($k_1 = 44.6\ \%, k_2 = 7.5\ \%, V_{\mathrm{core}} = 1.3V_{\mathrm{ref}}$)

(c) Conventional [3] ($k_1 = 40.3\ \%, k_2 = 0.3\ \%, V_{\mathrm{ref}} = 2.68 \times 10^{-4}\ \mathrm{m}^3$)

Fig. 5. Optimized and conventional WPT cores

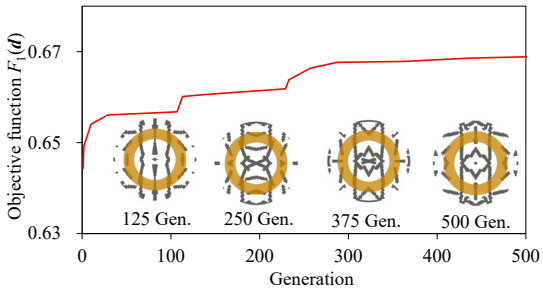

(a) Geometry projection

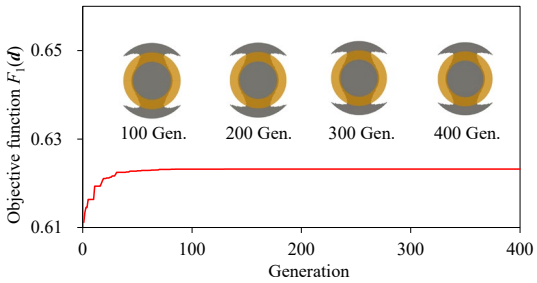

(b) NGnet

Fig. 6. Convergence histories of geometry projection method and NGnet

IV. Optimization Results

A. *Single-Objective Optimization: Problem 1*

We solve Problem 1 in (8). The optimization model of a WPT device is shown in Fig. 3, and Table I summarizes its specifications, where the leakage flux evaluation area is set based on the human exposure model to magnetic fields [15]. A WPT device is required to maintain good performance against misalignment. Here, we assume a significantly large misalignment that has a radius of Ω_{core}, as shown in Fig. 3 (a), to evaluate robustness. However, the air gap length is fixed for simplicity, even when a misalignment exists. To evaluate the coupling coefficients, we analyze two FE models with and without misalignment. The distributions of the elementary bars and Gaussian functions are shown in Fig. 4. To shape the transmitting and receiving coils symmetrically along the x, y, and z directions, 16 elementary bars are uniformly deployed in the quarter domain of Ω_{core} in the geometry projection method. In contrast, 48 Gaussian basis functions are deployed in the quarter domain such that the number of unknowns in the NGnet method is equal to that in the geometry projection method. To solve the optimization problem presented in (8) using real-coded GA, 720 individuals were generated for the first generation and 192 children were generated from 49 parents in each generation. Under these conditions, approximately five days are required to obtain the optimization results using an Intel Xeon CPU (3.5 GHz, 32 threads).

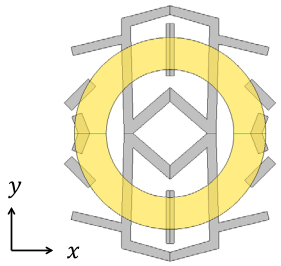

Fig. 7. Smoothed WPT core ($k_1 = 41.3\ \%, k_2 = 4.9\ \%, V_{\mathrm{core}} = 0.58V_{\mathrm{ref}}$)

The optimized and conventional WPT cores and their convergence histories are shown in Figs. 5 and 6, respectively. In addition, the coupling coefficients and core volumes are summarized in Fig. 5. The optimized core shapes depicted in Fig. 6 (b) plateau at 50 generations, whereas those shown in Fig. 6 (a) continue

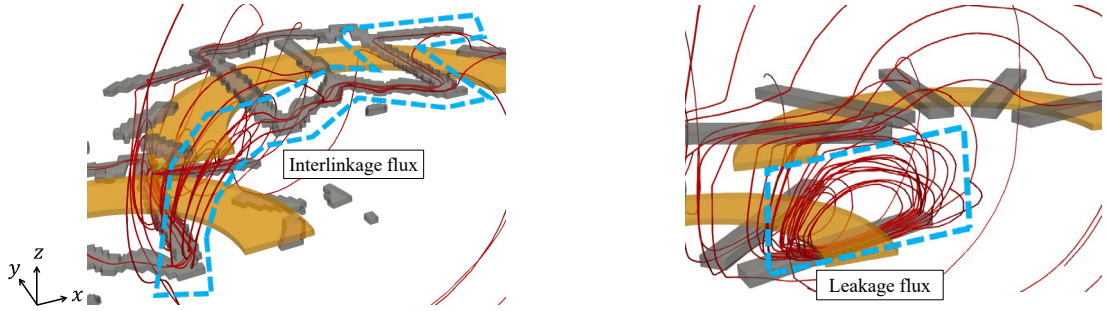

(a) Optimized solution to Problem 1 (Geometry projection) (b) Conventional

Fig. 8. Comparison of flux distributions with misalignment of 200 mm (1/2 fraction is shown)

to change such that the coupling coefficients increase. We can see that the optimized WPT cores shown in Fig. 5 (a) and (b) maintain relatively high coupling coefficient values against misalignment. However, it would be difficult to manufacture the optimized WPT core shown in Fig. 5 (b) when using the bar-shaped cores that are utilized in conventional WPT devices, as shown in Fig. 5 (c). In contrast, it would not be difficult to manufacture the optimized WPT core shown in Fig. 5 (a) using bar-shaped cores. The core volumes in Figs. 5 (a) and (b) are 35 % smaller and 30 % larger than the reference core volume shown in Fig. 5 (c), respectively. Although the optimized core shape shown in Fig. 5(a) is relatively simple, the cores have wavy surfaces, which might result in certain manufacturing difficulties unless they are smoothed. The smoothed WPT core shapes are shown in Fig. 7. We can see that the simplification of Fig. 5(a) has no significant effect on the performance. These results indicate that the geometry projection method is more suitable for the optimal design of WPT cores compared to the NGnet method.

To interpret the performance difference between the WPT cores depicted in Figs. 5 (a) and (c), their flux distributions with a 200 mm misalignment are comparatively shown in Fig. 8. The effective interlinkage flux from the transmitting coil to the receiving coil is shown in Fig. 8 (a). Leakage fluxes that pass through the magnetic cores can be observed in Fig. 8 (b).

B. Dependence on Optimization Parameters

To study the dependence of the convergence of the proposed method on hyperparameters, we perform optimizations under different conditions. The convergence histories of the proposed method, starting from different random seeds and different numbers of elementary bars, are shown in Fig. 9. The optimized WPT cores for different numbers of elementary bars are shown in Fig. 10. Note that the optimization results in Fig. 10 are obtained by utilizing uniformly deployed elementary bars in the quarter domain of Ω_{core}. We can see that the optimization results shown in Fig. 9 (a) indicate approximately constant performance regardless of the random seed, because the standard deviation, σ, among them is approximately 0.5 %. The number of elementary bars is found to have a relatively larger influence on the optimization results, as shown in Fig. 10.

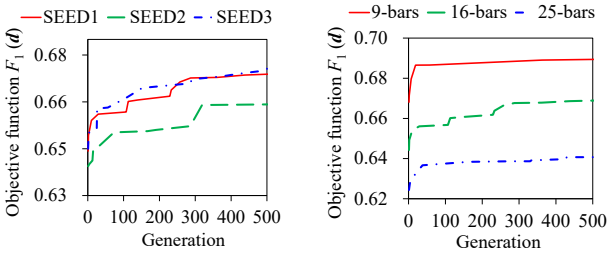

(a) Random seed (b) Number of elementary bars

Fig. 9. Dependence of hyperparameters on the convergence of GA

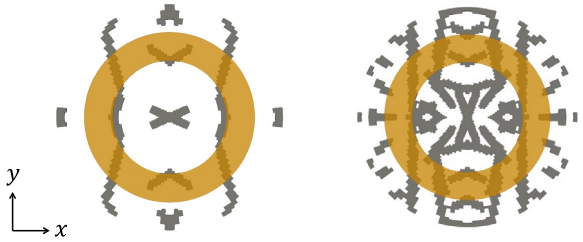

(a) 9 (3×3) bars
($k_1 = 34.3\ \%, k_2 = 5.5\ \%$, $V_{\text{core}} = 0.34V_{\text{ref}}$)

(b) 25 (5×5) bars
($k_1 = 42.2\ \%, k_2 = 7.2\ \%$, $V_{\text{core}} = 0.93V_{\text{ref}}$)

Fig. 10. Optimized WPT cores for different number of elementary bars, where Problem 1 is solved

C. Multi-Objective Optimization: Problem 2

We solve Problem 2 in (10). We again consider the optimization model shown in Fig. 4 (a). We use NSGA-II [16], where the number of individuals is set to 720, and the evolution process is continued for 1,000 generations. Approximately six days are required to obtain the optimization results using the Intel Xeon CPU (3.5 GHz, 32 threads).

The Pareto front at 1,000 generations and optimized WPT cores at representative points are shown in Fig. 11. We can see that the leakage flux of the Pareto solutions to Problem 2 is smaller than those of the conventional solution to Problem 1, whereas the coupling coefficient for the alignment case is not improved by solving Problem 2. The flux distributions and magnitude of the leakage flux densities for a misalignment of 200 mm are shown in Fig. 12. We find that optimized shape 1 has a large leakage flux. In contrast, the leakage flux of optimized shape 2 is relatively smaller than that of the other WPT cores. Thus, the Pareto solutions around

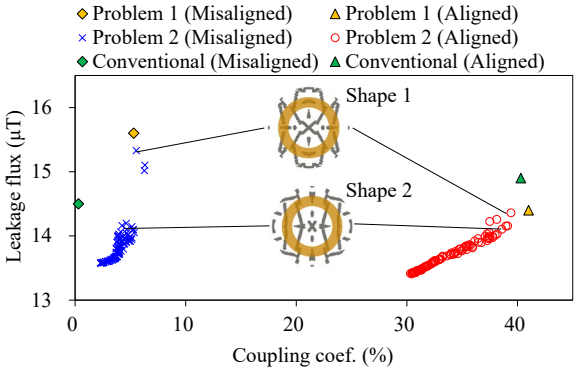

Fig. 11. Pareto front at 1,000 generation.

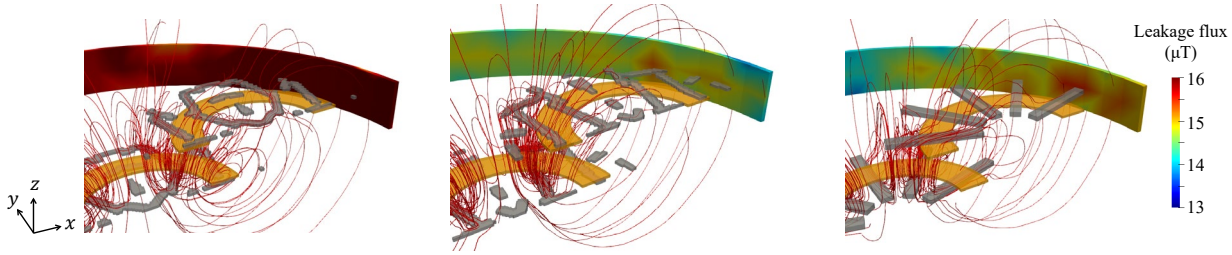

(a) Optimized shape 1 (Problem 2) ($k_2 = 5.5$ %, $B_2^{\text{leak}} = 15.3$ μT)

(b) Optimized shape 2 (Problem 2) ($k_2 = 4.6$ %, $B_2^{\text{leak}} = 14.2$ μT)

(c) Conventional ($k_2 = 0.3$ %, $B_2^{\text{leak}} = 14.5$ μT)

Fig. 12. Comparison of flux distributions on leakage flux evaluation area (1/2 fraction is shown)

optimized shape 2 have better performance than the conventional bar-shaped core shown in Fig. 5 (c) with respect to robustness and leakage flux.

V. Conclusion

In this study, we proposed a novel topology optimization method for the magnetic cores of WPT devices using the geometry projection method. We showed that the optimized core shape obtained by using the proposed method is robust against misalignment and more practical than that obtained by using NGnet. Moreover, the proposed method was applied to a multi-objective optimization case considering the coupling coefficients and leakage flux. The optimized bar-shaped core achieved by employing the proposed method has better performance than the conventional bar-shaped core with respect to robustness and leakage flux. In the future, we plan to manufacture optimized cores to verify their performance experimentally.

References

[1] M. Song, P. Belov, and P. Kapitanova, "Wireless Power Transfer Inspired by the Modern Trends in Electromagnetics," *Appl. Phys. Rev.*, vol. 4, Art. No. 021102, 2017.

[2] M. Budhia, G. A. Covic, and J. T. Boys, "Design and Optimization of Circular Magnetic Structures for Lumped Inductive Power Transfer Systems," *IEEE Trans. Power Electron.*, vol. 26, no. 11, pp. 3096-3108, 2011.

[3] L. Strauch, M. Pavlin, and V. B. Bregar, "Optimization, Design, and Modeling of Ferrite Core Geometry for Inductive Wireless Power Transfer," *IJAEM*, vol. 49, no. 1, pp. 145-155, 2015.

[4] T. Yilmaz, N. Hasan, R. Zane, and Z. Pantic, "Multi-Objective Optimization of Circular Magnetic Couplers for Wireless Power Transfer Applications," *IEEE Trans. Magn.*, vol. 53, no. 8, Art. no. 8700312, 2017.

[5] Y. Otomo and H. Igarashi, "A 3-D Topology Optimization of Magnetic Cores for Wireless Power Transfer Device," *IEEE Trans. Magn.*, vol. 55, no. 6, Art. no. 8103005, 2019.

[6] Y. Otomo and H. Igarashi, "3-D Topology Optimization of Magnetic Cores for Wireless Power Transfer with Double-Sided Winding Coils," *IJAEM*, vol. 60, no. S1, pp. S115-S123, 2019.

[7] Y. Gong, Y. Otomo, and H. Igarashi, "Multi-Objective Topology Optimization of Magnetic Couplers for Wireless Power Transfer," *IJAEM*, vol. 64, no. 1-4, pp. 325-333, 2020.

[8] J. A. Norato, B. K. Bell, and D. A. Tortorelli, "A Geometry Projection Method for Continuum-Based Topology Optimization with Discreate Elements," *Compt. Methods Appl. Mech. Eng.*, vol. 293, pp. 306-327, 2015.

[9] S. Zhang, A. L. Gain, and J. A. Norato, "A Geometry Projection Method for the Topology Optimization of Curved Plate Structures with Placement Bounds," *Int. J. Numer. Methods Eng.*, vol. 114, no. 2, pp. 128-146, 2018.

[10] S. Watts, D. A. Tortorelli, "A Geometry Projection Method for Designing Three-Dimensional Open Lattices with Inverse Homogenization," *Int. J. Numer. Methods Eng.*, vol. 112, no. 11, pp. 1564-1588, 2017.

[11] A. Komori, Y. Maki, M. Nakatsui, I. Ono, and M. Okamoto, "Efficient Numerical Optimization Algorithm Based on New Real-Coded Genetic Algorithm, AREX+JGG, and Application to the Inverse Problem in Systems Biology," *Applied Mathematics*, vol. 3, no. 10A, pp. 1463-1470, 2012.

[12] M. Chigira, *et al.*, "Small-Size Light-Weight Transformer with New Core Structure for Contactless Electric Vehicle Power Transfer System," in *Proc. IEEE ECCE*, pp. 260-266, 2011.

[13] M. Schlüter and M. Gerdts, "The Oracle Penalty Method," *J. Global Optimization*, vol. 47, pp. 293-325, 2010.

[14] L. Huang, *et al.*, "General Integral Formulation of Magnetic Flux Computation and Its Application to Inductive Power Transfer System," *IEEE Trans. Magn.*, vol. 53, no. 6, Art. no. 7001804, 2017.

[15] V. Cirimele, F. Freschi, L. Giaccone, L. Pichon, and M. Repetto, "Human Exposure Assessment in Dynamic Inductive Power Transfer for Automotive Applications," *IEEE Trans. Magn.*, vol. 53, no. 6, Art. no. 5000304, 2017.

[16] K. Dev, A. Pratap, S. Agarwal, and T. Meyarivan, "A Fast and Elitist Multiobjective Genetic Algorithm: NSGA-II," *IEEE Trans. Evol. Comput.*, vol. 6, no. 2, pp. 182-197, 2002.